ISSN (Print) : 0974-6846
ISSN (Online) : 0974-5645
Indian Journal of Science and Technology, *Vol 9(46), DOI: 10.17485/ijst/2016/v9i46/107139, December 2016*

Effect of Microwave Sintering Time and Homogenization Treatment on Biomedical Ti-51%Ni SMAs

Mustafa K. Ibrahim, E . Hamzah*, Safaa N. Saud, E. N. E. Abu Bakar and A. Bahador

Faculty of Mechanical Engineering, UniversitiTeknologi Malaysia, 81310 UTM Johor Bahru, Johor, Malaysia;
mustafakhaleel4@gmail.com,esah@fkm.utm.my, safaaengineer@gmail.com,
nazim@utm.my, A79bahador@gmail.com

Abstract

Objective: The influence of microwave sintering time and Homogenization Treatment (HT) on the microstructure, density, phase composition, mechanical properties and phase transformation temperatures of biocompatible Ti-51%Ni Shape Memory Alloys (SMAs) are determined. **Methods/Statistical Analysis**: These alloys are fabricated at 900˚C for two different sintering times such as 5 min. and 30 min. **Findings**: The Field Emission Scanning Electron Microscopy (FESEM) micrographs show microstructure of needle-like morphology except for the sample which sintered at 900˚C for 30 min. without HT. **Applications/Improvements:** Sample synthesized at 900˚C for 30 min. without HT revealed the highest performance in terms of maximum compressive strength (1376 MPa) at 29% strain, Austenite finish temperature (Af) of 27˚C and Martensite finish temperature (Mf) of 47˚C at 18% porosity. They showed the Af temperature very close to the human body temperature, thus prospective for biomedical applications. During heating, the Differential Scanning Calorimeter (DSC) baseline shows multi-endothermic peaks, while during the cooling process there is only one exothermic peak.

Keywords: Mechanical Properties, Microstructure, Powder Metallurgy, Ti-51%Ni SMAs

1. Introduction

Shape Memory Alloys (SMAs) appear prospective for diverse applications due to their distinct thermo-mechanical coupling over a broad range of fields. Besides, biomedical Shape Memory Alloys (SMAs) must possess stable shape memory property, biocompatibility and superior corrosion resistance. Amongst all the Shape Memory Alloys, Ti-51%Ni is most successful towards the construction of novel medical implants. However, the biocompatibility, toxicity, carcinogenic effects and allergenic properties of Ni being the major concern needs improvement[1]. Ti-Ni alloys acquiring all these attributes are extensively applied for biomedical purposes including joints replacement, dental implants, stents, fusion cages, mechanical valves, etc[2–5]. The super-elasticity and shape memory effects of Ti-Ni alloys are greatly decided by their martensitic transformation. These alloys must match the characteristics of the living tissues, whenever used at the temperature of the human body[6].

Titanium-Nickel (Ti-Ni) alloys produced via Powder Metallurgy (PM) provide near-net shape products, which do not require machining and/or deformation operations[7–11]. Six Powder Metallurgy methods are developed to fabricating the dense or porous Ti-Ni alloys from elemental and/or pre-alloyed powders such as Spark Plasma Sintering (SPS)[12], Hot Isostatic Pressing (HIP) for sintering materials at elevated pressure[13], cold pressing and sinter-

*Author for correspondence

ing or Conventional Sintering (CS)[14], Self-Propagating High Temperature Synthesis (SHS)[15,16], Metal Injection Molding (MIM)[17,18] and Microwave Sintering (MWS)[19,20]. In this category, microwave sintering is relatively a newer fabrication method[19–21] and greatly advantageous due to time and energy economy, enhanced diffusion process, rapid heating rates, as well as improved mechanical and physical properties[22,23]. Considering these notable benefits of microwave sintering method, we examine the effect of sintering time and Homogenization Treatment on the microstructure, mechanical properties and phase transformation temperatures of microwave sintering grown Ti-51%Ni Shape Memory Alloys useful for biomedical applications.

2. Materials and Methods

Ti particles of diameter 150 μm (99.5% purity) are mixed with Ni particles of diameter 45 μm (purity 99.5+ %) in a planetary ball mill (PM100) for 1 h at the speed of 300 rpm with rest of 10 min. For each 20 min milling, the ball to powder weight ratio is selected as 4:1. Analytical grade Ti and Ni are supplied by Goodfellow Cambridge Limited, Huntingdon, PE29 6WR, England. Ti-51%Ni powders are then cold-pressed to green samples of size (Φ15 × 6 mm) under a uniaxial pressure of 230 kg/cm^2 for 5 min. followed by MWS (type, HAMiLab-V3, SYNOTHERM Corp.) sintering machine. Samples are sintered at 900˚C for 5 min and 30 min with the heating rate of 30˚C/min. followed by Homogenization Treatment (HT) for 30 min and water quenching. Then, the samples are machined to dimensions of (4 mm × 4 mm × 8 mm) according to the ASTM E9-09 standards. Electrical Discharge Machining (EDM) wire cut is employed to analyzing the microstructure, X-ray Diffraction and compressibility. These samples are coupled with microwaves and allowed them to transfer the heat to adjusting the sintering temperature.

Figure 1 shows the microwave sintering insulation barrel that is continuously operated at 2.45 GHz and 4.5 kV. The sintering is performed under argon gas (99.999% purity) atmosphere. The compacts are placed in alumina crucible surrounded by Silicon Carbide (SiC) particles located at the crucible corners, where SiC served as auxiliary heat material. The samples temperature during sintering are measured using infrared pyrometer as indicated.

The microstructures of samples are imaged using Field Emission Scanning Electron Microscope (FESEM,

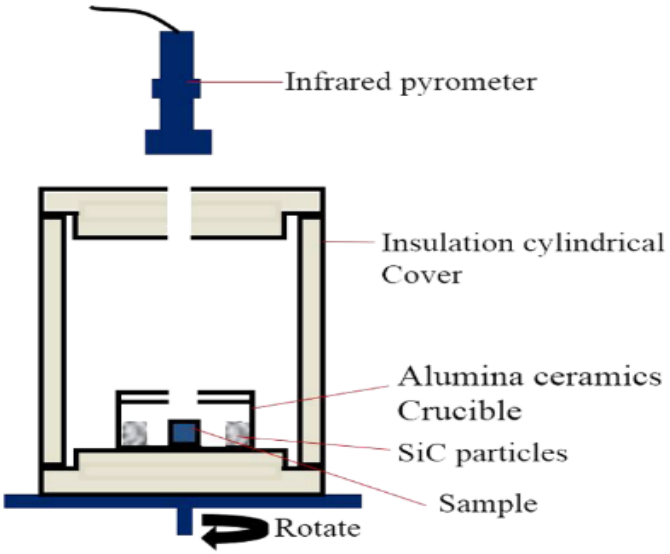

Figure 1. Schematic diagram of MWS insulation barrel.

Zeiss-LEO Model 1530). Nikon optical microscopy is used to identify the influence of sintering time and HT on the pores size, pores shape and pores distribution of Ti-51%Ni samples. The pores size, shape and distribution are analyzed using "isolution lite" software. The samples density is measured using Archimedes drainage principle. The phase compositions and lattice planes of Ti-51%Ni samples are determined using D5000 Siemens X-ray diffractometer (fitted with CuKα X-ray source) interfaced with jade software, the scanning mode was locked couple, scan rate of 0.05 o/sec and 2θ range between 20-90˚. The compression test is performed on Instron 600 DX-type universal machine with constant speed of 0.5 mm/min, at 25˚C. Vickers hardness test is carried out (Matsuzawa Vicker) with 30 kg force kept for 20 s at an ambient temperature of 25˚C. The Differential Scanning Calorimeter (DSC 8500, PerkinElmer) is used to determine the phase transformation temperatures of these alloys, which is interfaced with Pyris software under heating/cooling rates of 10˚C/min. The sintering time was 5 min. and 30 min. because we like to investigate the effect of sintering time at short and long sintering time, while the using of 900˚C as sintering temperature was because the increasing of the sintering temperature much more than the transformation temperature (882˚C) of titanium reduces the shape memory effect of titanium alloys, the sintering at temperature more than the transformation temperature is necessary in order to provide the martensitic transformation due to cooling from austenitic structure above (882˚C) to martensitic structure (at low temperature depends on the type of materials).

3. Results and Discussion

3.1 Microstructure Characterization

Figure 2 (a-d) shows the optical micrographs to illustrate the effect of sintering time and Homogenization

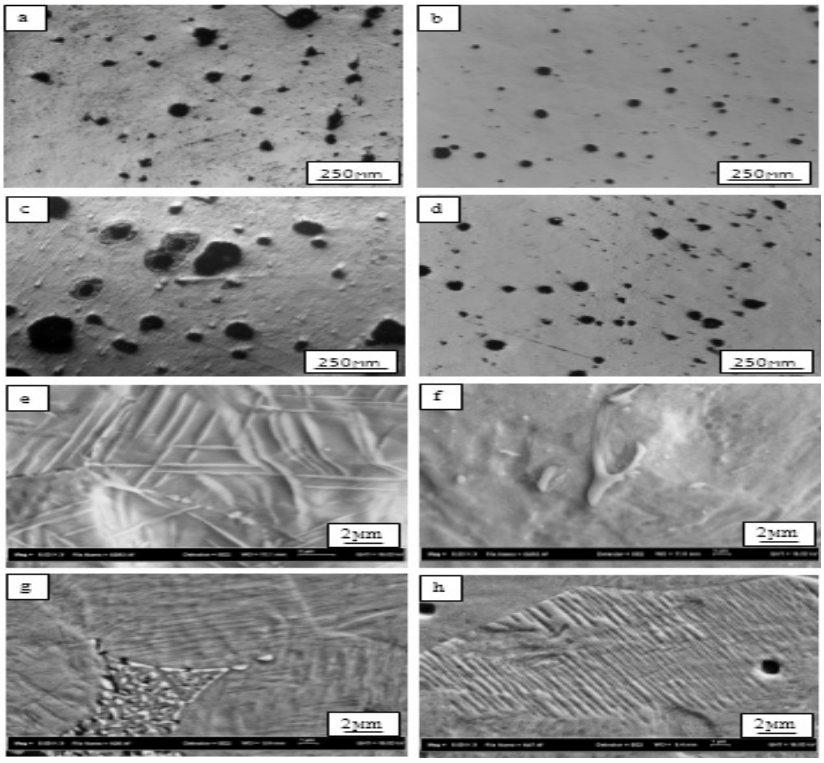

Figure 2. Field Emission Scanning Electron Microscopy (FESEM) and optical micrographs of Ti-51%Ni Shape Memory Alloys sintered at 90 ˚C for (a and e) 5 min, (b and f) 30 min, (c and g) 5 min, followed by HT at 900˚C for 30 min. and water quenching and (d and h) 30 min, followed by HT at 900˚C for 30 min and water quenching.

Treatment (HT) on the pores size and pores distribution of Ti-51%Ni samples. The pores size is found to decrease with the increase of sintering time. Conversely, the HT enhanced the pores size. The occurrence of in-homogenized distribution of the pores in these samples is attributed to the faster diffusion of Ni than Ti. This clearly demonstrates that the Ni diffusion from the Ni-rich region is higher than that of the Ti from the Ti-rich region. Furthermore, this difference in diffusion rate caused vacancies in the Ni-rich regions[24,25]. Figure 2 (e-h) displays the Field Emission Scanning Electron Microscopy FE-SEM micrographs of the microstructures of microwave sintered Ti-51%Ni samples. These samples are sintered at 900˚C for 5 min. and 30 min. For 5 min sintering duration without HT, the β-martensitic needles are formed. These β-martensitic needles are generated after HT with sintering time of 5 min. and 30 min. The complete absence of martensitic needles at sintering time of 30 min. before homogenization is ascribed to the prolonged sintering duration, which required faster cooling rate. The grain boundaries are clearly evidenced in post-homogenization treated samples, where the martensitic needles appeared longer and dense with same orientation inside the grain. Moreover, before homogenization for 5 min sintering time, the martensitic needles appeared sharper with multi-orientations but weakly dense. All samples are etched for same duration using a solution composed of 10%HF-40%HNO_3-50% distilled water.

Figure 3 depicts the mapping of Ti-51%Ni alloy sintered at 900˚C for 5 min. after Homogenization Treatment. The distribution of Ti and Ni in this SMA is discerned to be close to the real composition of Ti and Ni elements. Table 1 enlists the pores size, relative density and Vickers hardness of Ti-51%Ni SMAs. After homogenization treatment, the average range of pores size range is increased.

Figure 4 illustrates the X-Ray Diffraction (XRD) patterns of fabricated Ti-51%Ni samples sintered at 900˚C for 5 min and 30 min before and after homogenization treatment. These samples exhibited B2 and B19′ phases with few secondary phases of $TiNi_3$ and Ti_2Ni because of the porosity lower than 20%. The TiNi alloys are formed through the primary reaction between Ti and Ni or secondary weak reactions among Ti_2Ni, $TiNi_3$, Ti, and Ni.

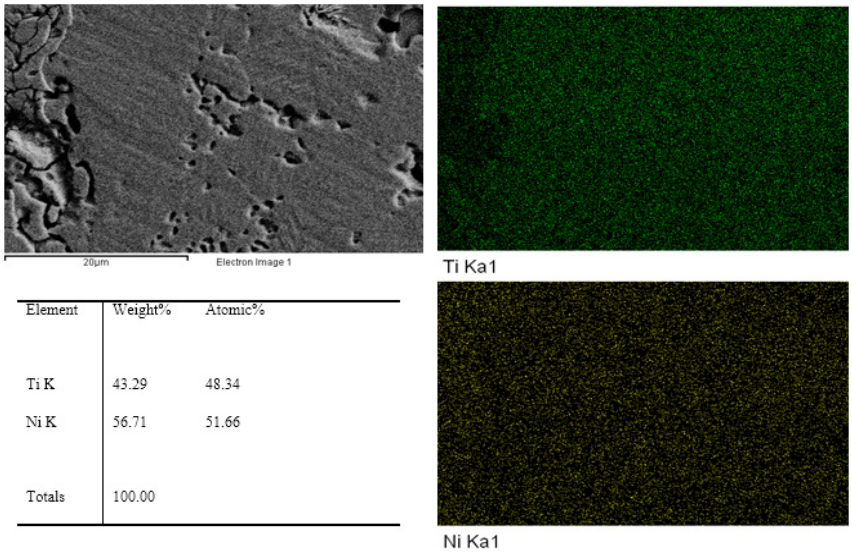

Element	Weight%	Atomic%
Ti K	43.29	48.34
Ni K	56.71	51.66
Totals	100.00	

Figure 3. Mapping of Ti-51%Ni SMA sintered at 900˚C for 5 min. after HT at 900˚C for 30 min. and water quenching.

Table 1. Pores size, relative density and Vickers hardness of Ti-51%Ni shape memory alloys. (ρ) is the measured density of the fabricated sample and (ρ0) is the theoretical density of Ti-Ni alloy

MWS parameters	Pores size range (μm)	Average pores size (μm)	Relative density (ρ/ρ0)%	Vickers hardness (Hv)
900 ˚C and 5 min	<10-70	38	83.5	157
900 ˚C and 30 min	<10-30	17	87	105
900 ˚C and 5 min, followed by HT	<10-136	57	82.2	104
900 ˚C and 30 min, followed by HT	<10-54	39	84	100

The TiNi alloys that are formed via primary reaction of Ti and Ni are thermodynamically unfavorable[20]. In[26] acknowledged that $TiNi_3$ and Ti_2Ni are formed via thermodynamically favorable solid-state reaction. The XRD pattern revealed crystalline peaks corresponding to the B2 phase grown along the lattice planes of (211), (200), (220) and (110) at 78˚, 61.5˚, 53˚ and 41.5˚ angles, respectively. The crystalline peaks corresponding to the B19′ phase grown along the direction of (-112), (012), (-111) and (002) lattice are matched to the angles of 53˚, 44.8˚, 41˚ and 38.5˚, respectively. The crystalline peaks corresponding to the Ti_2Ni phase grown along the lattice direction

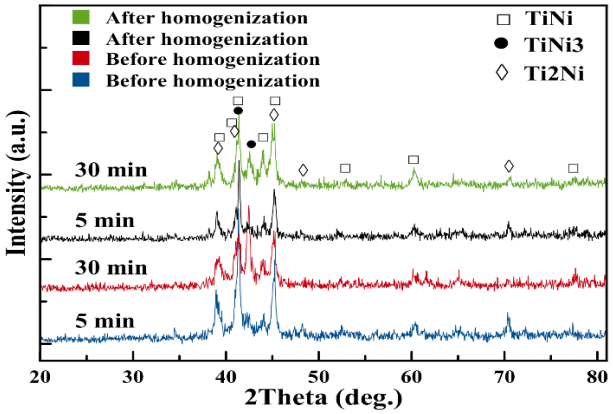

Figure 4. XRD patterns of Ti-51%Ni SMAs sintered at 900˚C.

of (822), (442), (440), (511) and (422) are matched to the angles of 70˚, 48˚, 45˚, 41˚ and 38˚, respectively. Meanwhile, the crystalline peaks corresponding to the $TiNi_3$ phase grown along the lattice direction of (004) and (110) are matched to the angles of 43˚ and 41.5˚, respectively[20,27–29].

3.2 Stresses-Strain Curves

Figure 5 demonstrates the compressive properties of Ti-51%Ni SMAs sintered at 900˚C for 5 min. and 30 min, before and after Homogenization Treatment (HT). In the initial stages, the compressive curves showed lower slope for the sample which are sintered for 30 min. before HT than the one which are sintered for 5 min. after Homogenization Treatment. This observation is attributed to the experimental artifact or instrumental errors. By ignoring these initial stages, the compressive curves can be divided into three regions[30]. The first region is a linear elastic deformation region, where the slope corresponds to the elastic modulus of the alloy. The second region is a plastic yield deformation region, which manifested the samples compressive strength as a peak stress. The third region signifies the rupture region.

The elastic modulus of the samples sintered for 5 min. and 30 min. before HT are determined to be 6.62 and 6.6 GPa, respectively. Conversely, after HT this elastic modulus is increased to 8.1 and 9 GPa, respectively. Furthermore, the highest maximum strength of the sample sintered for 30 min. before HT is measured to be 1376 MPa at strain 29%. Meanwhile, the sample which is sintered for 5 min. revealed the maximum strength of 1170 MPa at strain 27%. The same sample which is sintered for 30 min. but after HT exhibited a lowering in the maximum strength as well as strain (1000 MPa at strain 11.5%). The sample which is sintered for 5 min. but after HT exhibited a diminished maximum strength of 660 MPa at strain 7.5%. This observed reduction in the maximum strength and strain after HT is majorly attributed to the increase in samples elastic modulus, which appeared to be more brittle.

3.3 Transformation Temperatures

Figure 6 presents the Differential Scanning Calorimeter (DSC) curves of Ti-51%Ni SMAs sintered at 900˚C for 5 min. and 30 min. with and without Homogenization Treatment. During samples heating (without Homogenization Treatment) a multi-step phase transformation is evidenced, where B19′ phase first underwent a transformation to R and then to B2. The presence of such R phase in these alloys is reported earlier[31–33], where these

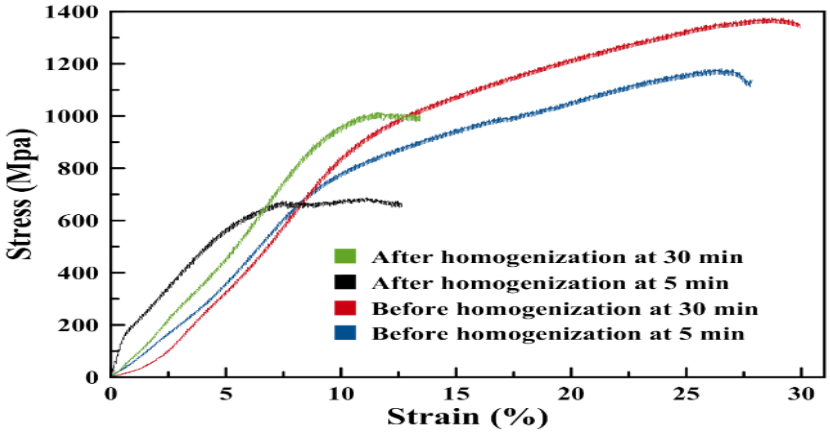

Figure 5. Compression curves of Ti-51%Ni SMAs sintered at 900˚C.

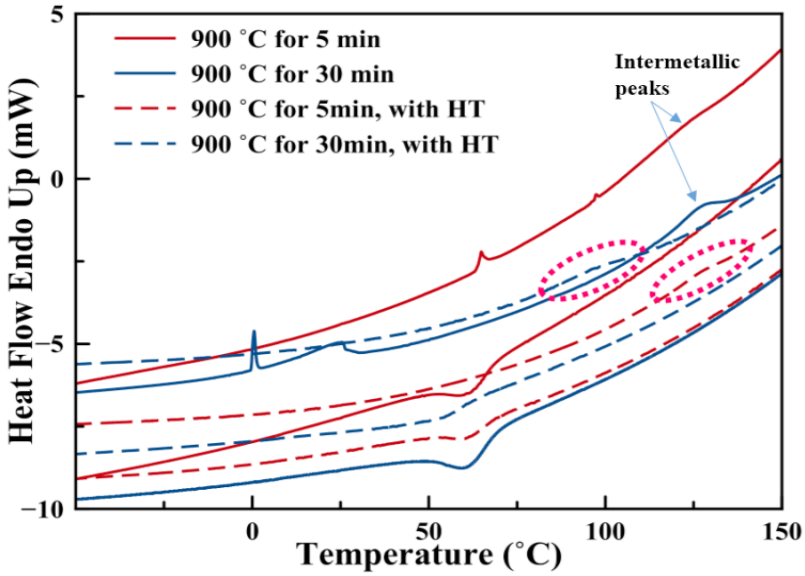

Figure 6. Differential Scanning Calorimeter (DSC) curves of Ti-51%Ni SMAs sintered at 900˚C for 5 and 30 min. with and without homogenization heat treatment.

Table 2. Transformation temperatures of Ti-51%Ni SMA with different sintering parameters

MWS parameters	Rs (˚C)	Rf (˚C)	As (˚C)	Af (˚C)	Ms (˚C)	Mf (˚C)	Mp (˚C)
900 ˚C and 5 min	62.5	67	95.5	98.6	69.2	52.7	59.6
900 ˚C and 30 min	-0.3	2.1	3.2	27	69	47	60.1
900 ˚C and 5 min, with HT	—	—	102	139.5	69.6	50.5	60.5
900 ˚C and 30 min, with HT	—	—	69	114	63	40	60.5

samples revealed intermetallic peaks. An increase in the sintering time from 5 min. to 30 min. caused a reduction of Austenite start temperature (As) and Austenite finish temperature (Af). This decrease allowed the Af to remain more closer to the human body temperature. Thus, the samples with sintering time of 30 min. are considered to be the appropriate one for biomedical applications. After homogenization heat treatment these samples displayed an endothermic peak, which is assigned to the B19′ to B2 phase transformation during heating. Moreover, after homogenization heat treatment and during heating process the values of As and Af are found to increase for both samples compared to those obtained without homogenization. These intermetallic peaks are marked by dotted pink circle in the diagram. During cooling of these samples with and without homogenization heat treatment, only one exothermic peak is observed which is allocated to B2 to B19′ phase transformation. During cooling, all samples showed nearly the same values of Martensite start temperature (Ms) and Martensite finish temperature (Mf).

However, only the sample sintered for 30 min followed by HT displayed slightly lower Ms and Mf values. Table 2 summarizes the transformation temperatures of sintered Ti-51%Ni SMAs before and after HT.

4. Conclusion

Using microwave sintering technique was successfully fabricated the Ti-51%Ni SMAs. The effects of microwave sintering time and Homogenization Treatment on the microstructure, density, composition, mechanical properties and phase transformation temperatures of these as synthesized alloys are reported. Small pores sizes are achieved at longer sintering time of 30 min. Needle-like microstructure of Ti-51%Ni SMAs are evidenced. However, before homogenization and at 30 min. sintering time these needle-like microstructure are disappeared even in the presence of same phase composition. The highest stress-strain is attained for the sample which is sintered at temperature 900˚C for 30 min. duration. They showed the Af temperature as very close to the human body temperature, thus prospective for biomedical applications. Our systematic methods for sample preparation and characterization may constitute a basis for the production of good quality biocompatible Ti-51%Ni SMAs.

5. Acknowledgment

The authors thank the Ministry of Higher Education of Malaysia and University Technology Malaysia for providing the financial support under the University Research Grant No. Q.J130000.3024.00M57 and research facilities.

6. References

1. Biesiekierski A, Wang J, Gepreel MA-H, Wen C. A new look at biomedical Ti-based shape memory alloys. Acta biomaterialia. 2012; 8(5):1661–9.
2. Oshida Y, Sachdeva R, Miyazaki S. Micro analytical characterization and surface modification of TiNi orthodontic archwires. Bio-medical Materials and Engineering. 1991; 2(2):51–69.
3. Duerig TW, Melton K, Stockel D. Engineering aspects of shape memory alloys: Butterworth-Heinemann; 2013.
4. Miyazaki S, Otsuka K. Development of shape memory alloys. ISIJ International. 1989; 29(5):353–77.
5. Mishnaevsky L, Levashov E, Valiev RZ, Segurado J, Sabirov I, Enikeev N. Nanostructured titanium-based materials for medical implants: Modeling and development. Materials Science and Engineering: R: Reports. 2014; 81:1–19.
6. Skorentsev L, Demidenko V. Energy difference and energy of mixing for crystalline structures of Ni-Ti-Mo alloys. Russian Physics Journal. 1995; 38(6):579–83.
7. Hey J, Jardine A. Shape memory TiNi synthesis from elemental powders. Materials Science and Engineering: A. 1994; 188(1):291–300.
8. Zhang N, Khosrovabadi PB, Lindenhovius J, Kolster B. TiNi Shape Memory Alloys prepared by normal sintering. Materials Science and Engineering: A. 1992; 150(2):263–70.
9. Green S, Grant D, Kelly N. Powder metallurgical processing of Ni–Ti shape memory alloy. Powder metallurgy. 1997; 40(1):43–7.
10. Igharo M, Wood J. Compaction and sintering phenomena in titanium-nickel shape memory alloys. Powder Metallurgy. 1985; 28(3):131–9.

11. Morris D, Morris M. Ni-Ti intermetallic by mixing, milling and interdiffusing elemental components. Materials Science and Engineering: A. 1989; 110:139–49.
12. Zhao Y, Taya M, Kang Y, Kawasaki A. compression behavior of porous Ni-Ti shape memory alloy. Acta materialia. 2005; 53(2):337–43.
13. Bertheville B, Neudenberger M, Bidaux JE. Powder sintering and shape-memory behavior of NiTi compacts synthesized from Ni and TiH2. Materials Science and Engineering: A. 2004; 384(1):143–50.
14. Li BY, Rong LJ, Li YY. Porous NiTi alloy prepared from elemental powder sintering. Journal of Materials Research. 1998; 13(10):2847–51.
15. Zanotti C, Giuliani P, Terrosu A, Gennari S, Maglia F. Porous Ni–Ti ignition and combustion synthesis. Intermetallics. 2007; 15(3):404–12.
16. Li BY, Rong LJ, Li YY, Gjunter V. A recent development in producing porous Ni–Ti shape memory alloys. Intermetallics. 2000; 8(8):881–4.
17. Aust E, Limberg W, Gerling R, Oger B, Ebel T. Advanced bone screw implant fabricated by metal injection moulding. Advanced Engineering Materials. 2006; 8(5):365–70.
18. Benson J, Chikwanda H. The challenges of titanium metal injection moulding. Journal for New Generation Sciences. 2009; 7(3):1–14.
19. Xu J, Bao L, Liu A, Jin X, Tong Y, Luo J, et al. Microstructure, mechanical properties and super elasticity of biomedical porous NiTi alloy prepared by microwave sintering. Materials Science and Engineering: C. 2015; 46:387–93.
20. Tang C, Zhang L, Wong C, Chan K, Yue T. Fabrication and characteristics of porous Ni-Ti shape memory alloy synthesized by microwave sintering. Materials Science and Engineering: A. 2011; 528(18):6006–11.
21. Tang C, Wong C, Zhang L, Choy M, Chow T, Chan K, et al. In situ formation of Ti alloy/TiC porous composites by rapid microwave sintering of Ti6Al4V/MWCNTs powder. Journal of Alloys and Compounds. 2013; 557:67–72.
22. Oghbaei M, Mirzaee O. Microwave versus conventional sintering: A review of fundamentals, advantages and applications. Journal of Alloys and Compounds. 2010; 494(1):175–89.
23. Das S, Mukhopadhyay A, Datta S, Basu D. Prospects of microwave processing: An overview. Bulletin of Materials Science. 2009; 32(1):1–13.
24. Sadrnezhaad SK, Lashkari O. Property change during fixtured sintering of Ni-Ti memory alloy. Materials and Manufacturing Processes. 2006; 21(1):87–96.
25. Zhu S, Yang X, Hu F, Deng S, Cui Z. Processing of porous TiNi shape memory alloy from elemental powders by Ar-sintering. Materials Letters. 2004; 58(19):2369–73.
26. Laeng J, Xiu Z, Xu X, Sun X, Ru H, Liu Y. Phase formation of Ni-Ti via solid state reaction. PhysicaScripta. 2007; 2007(T129):250.
27. Yang L, Tieu A, Dunne DP, Huang S, Li H, Wexler D. Cavitation erosion resistance of Ni-Ti thin films produced by Filtered Arc Deposition. Wear. 2009; 267(1):233–43.
28. Chu Cl, Chung JC, Chu PK. Effects of heat treatment on characteristics of porous Ni-rich NiTi SMA prepared by SHS technique. Transactions of Nonferrous Metals Society of China. 2006; 16(1):49–53.
29. Dovchinvanchig M, Zhao C, Zhao S, Meng X, Jin Y, Xing Y. Effect of Nd addition on the microstructure and Martensitic transformation of Ni-Ti shape memory alloys. Advances in Materials Science and Engineering. 2014; 2014:1–6.
30. Gao Z, Li Q, He F, Huang Y, Wan Y. Mechanical modulation and bioactive surface modification of porous Ti–10Mo alloy for bone implants. Materials and Design. 2012; 42:13–20.
31. Mentz J, Frenzel J, Wagner MF-X, Neuking K, Eggeler G, Buchkremer HP, et al. Powder metallurgical processing of Ni-Ti Shape Memory Alloys with elevated transformation temperatures. Materials Science and Engineering: A. 2008; 491(1):270–8.
32. Yuan B, Zhang X, Chung C, Zhu M. The effect of porosity on phase transformation behavior of porous Ti–50.8 at. % Ni Shape Memory Alloys prepared by capsule-free hot isostatic pressing. Materials Science and Engineering: A. 2006; 438:585–8.
33. Su P, Wu S. The four-step multiple stage transformation in deformed and annealed Ti49Ni51 shape memory alloy. Acta materialia. 2004; 52(5):1117–22.